ACS OMEGA

Open Access

http://pubs.acs.org/journal/acsodf

Article

The Role of Spacer Segments in Increasing the Transfection Efficacy of Au-Core Polymeric-Shell Nanoparticulate Gene Vectors

Denisse I. Bostiog,[#] Valentin Nastasa,[#] Cristina M. Al-Matarneh,[*] Dragos Peptanariu, Mihai Mares, Sorin A. Pasca, Andra C. Bostanaru-Iliescu, Bogdan F. Craciun, Tudor Vasiliu, Razvan Puf, Stelian S. Maier, and Mariana Pinteala[*]

Cite This: *ACS Omega* 2026, 11, 4430−4439

Read Online

ACCESS | Metrics & More | Article Recommendations | Supporting Information

ABSTRACT: The surface chemistry of gold nanoparticles is a key determinant of their final biological properties. In this study, we investigated the influence of the PEG chain length, positioned between the gold core and the cationic polymer, on the transfection efficiency in HeLa and HGF cell lines. Two types of nonviral vectors were synthesized from the same AuNPs, which were subsequently functionalized with PEG of 1000 and 2500 Da, respectively. Onto these PEG chains, identical copolymeric sequences of PEI2000-PEG500-GA were covalently attached to provide quasi-shielding (via PEG500) and enable tumor targeting/accumulation (via GA). Both vectors demonstrated that such functionalization enhances cellular uptake and targeting specificity while exhibiting excellent DNA delivery efficiency, minimal *in vitro* cytotoxicity, and no detectable *in vivo* adverse effects following intravenous administration in animal models. A superior loading capacity was observed when the PEG linked to the gold core was 2500 Da, suggesting a contribution from solvation-driven interactions.

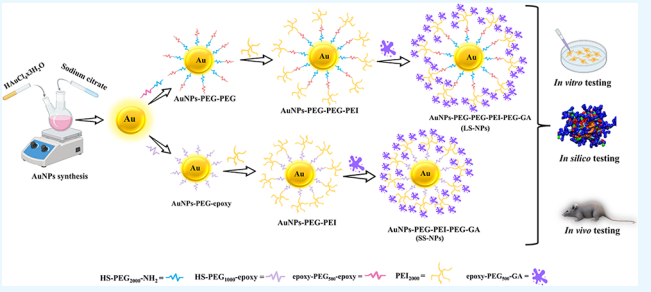

INTRODUCTION

Gene therapy is expected to play a pivotal role as a technique for cell reprogramming,[1] with potential applications for controlling malignant progression by immunotherapy,[2] or even for reversion of tumors to the benign state.[3] Essentially, gene therapy involves the controlled introduction into target eukaryotic cells of segments of exogenous nucleic acids carrying relevant information for reprogramming some of the normal or pathological intracellular molecular mechanisms.[4] The method applied for this purpose is called transfection. It is practiced either through relatively aggressive physical−chemical processes against cells, such as electroporation, or through carrier-mediated transfer processes, which minimally affect the integrity of living cells.[5] Even though variants of transfection have already reached the stage of clinical trials,[6,7] there still exists an objective factor that delays the development of spectacular applications of cellular reprogramming, especially *in vivo*, which is the lack of transfection molecular tools capable of cumulatively fulfilling five criteria: (i) low negative impact, if any, on nontargeted cells, (ii) minimal or at least slow immune system response, (iii) reproducibility of their intended action, (iv) ability to transfer large-enough segments of nucleic acids, and (v) high efficacy of the transfer of nucleic acids into cells. Of the two classes of molecular tools (usually called gene vectors), viral and nonviral, the latter seems to promise higher safety in use in gene therapy,[8,9] being preferable even if, to date, they are less efficacious.

Being of real relevance in modern transfection techniques, nonviral gene vectors with complex molecular and/or nanoparticulate architectures are currently expanding,[10] both through design and through performance studies. In terms of design, nanoparticles capable of generating polyplexes (spontaneously self-assembled noncovalent complexes, predominantly based on electrostatic interactions) with nucleic acids are favored, as they can collectively contribute to the firm and tight packaging of large segments of polynucleotides. This is the reason why most nonviral vectors possess peripheral shells made up of macromolecules that are positively charged in the physiological/pathological environment,[11] such as branched polyethylenimines (b-PEIs). The rigor and reproducibility of polyplex packaging increase, and implicitly, the transfection efficiency improves, if the shell adopts a systematic omnidirectional spatial organization (a compact but adjustable spheroidal geometry)[12] and an extended and unrestrained

Received: September 29, 2025
Revised: December 10, 2025
Accepted: December 31, 2025
Published: January 14, 2026

https://doi.org/10.1021/acsomega.5c10142
ACS Omega 2026, 11, 4430−4439

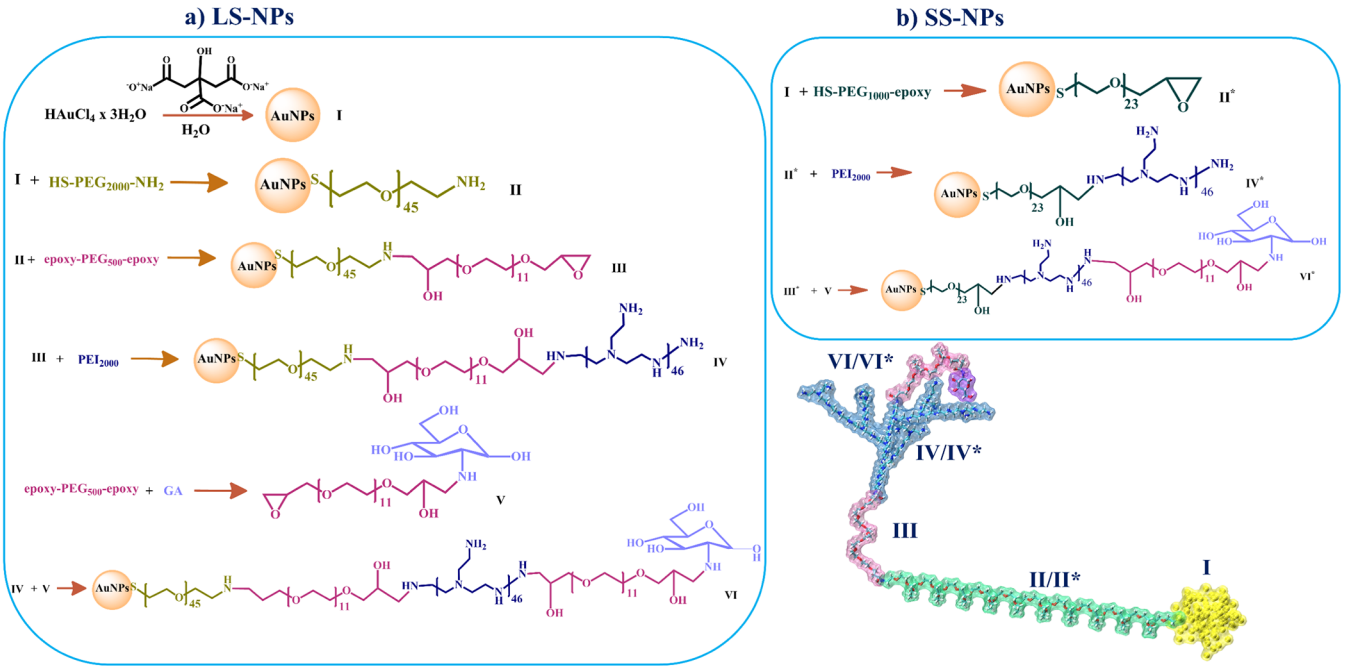

Figure 1. Steps of the synthesis of polysegmented chains of the core−shell nanoparticles acting as nonviral gene vectors.

("relaxed") spatial distribution of its macromolecular segments. The firmness of the omnidirectional symmetry can be ensured by the core−shell architecture of nanoparticles (possibly with a metallic core), while the "relaxed" spatial distribution may come from the length and the polysegmental structure of the chains grafted onto the core. In this context of the design of nonviral gene vectors, the present paper is focused on demonstrating that the insertion of spacer segments made of weakly reactive macromolecules, such as poly(ethylene glycols), into the grafted chains can improve the transfection efficiency of novel nanoparticulate delivery systems, as a consequence of the enhanced segmental mobility of their chains, allowing the vectors to intimately "palpate" the polynucleotide chains and to adapt dynamically to their local conformation. Due to the polysegmental structure of their molecular chains, nanoparticles are prone to dynamically interact both with the payload and with each other to "collaborate" in their role as nonviral gene vectors. The effectiveness of such vectors is therefore a matter of chemical functionality, flexibility, and long-range spatial adaptability of their (macro)molecular chains. All three mentioned characteristics (functionality, flexibility, adaptability) were considered both when designing the (macro)molecular structure of the chains that make up the shell and when designing the steps of synthesis of nanoparticles.

Safety of administration and operation is an essential parameter in the design of a delivery system, including in the case of gene vectors, especially if they act in a nanoscale state, when they could trigger cytotoxic processes.[13,14] Prevention of excessive spread and uncontrolled action of engineered nanoparticles in living organisms must always be considered. This is why, regardless of their chemical composition and supramolecular morphology,[15] modern nanoparticulate delivery systems are endowed with targeting molecules capable of identifying peculiar biochemical species and/or tissue-specific milieus,[16] or at least promoting accumulation in peculiar cells or tissues.[17] The accumulation of nanoparticles in tumor tissue can be mediated by their decoration with molecules identical to or similar to those intensely involved or consumed in the metabolism of neoplastic cells. As a precursor in protein glycosylation processes, glucosamine (GA), an aminosaccharide, is significantly consumed by rapidly dividing tumor cells. This fact suggests that, when used as a decorating agent, GA may function as a promoter of the accumulation of particulate nonviral vectors in tissues undergoing accelerated dimensional expansion. Consequently, this small molecule was selected to functionalize the nanoparticles with a carbohydrate-based periphery during their development.

The polysegmental organization of the macromolecular chains, together with their grafting density on the core, offers increased versatility for the spatial structuring of the nanoparticle shell.

To demonstrate the impact of this fact on transfection efficiency and starting from our previous achievements in the realm of nonviral gene vectors,[18−20] the present study describes the design and synthesis of two new classes of nanoparticulate carriers having complex shells based on polymer segments in the following sequences: (i) **PEG_{2000}-PEG_{500}**-PEI_{2000}-PEG_{500}-GA and (ii) **PEG_{1000}**-PEI_{2000}-PEG_{500}-GA, for which the differences are marked in bold italics. These macromolecular sequences were successfully synthesized onto the surface of gold nanoparticles (AuNPs) in a layer-by-layer grafting manner. Subsequently, the new carriers were evaluated as potential facilitators of both gene delivery and cell targeting. The design and selection for application purposes (as gene vectors or as theranostic drug carriers) of the polymeric sequences rely on our observation that peculiar molecular architectures of PEG, PEI, and GA derivatives have demonstrated the ability to improve the transfection efficiency. To summarize, we designed and synthesized core−shell nanoparticles with a core of gold atoms and a polymeric shell composed of chains arranged in the following sequence: (i) a highly flexible PEG spacer grafted onto the core, (ii) a polycationic PEI segment acting as an electrostatic linker for

https://doi.org/10.1021/acsomega.5c10142
ACS Omega 2026, 11, 4430−4439

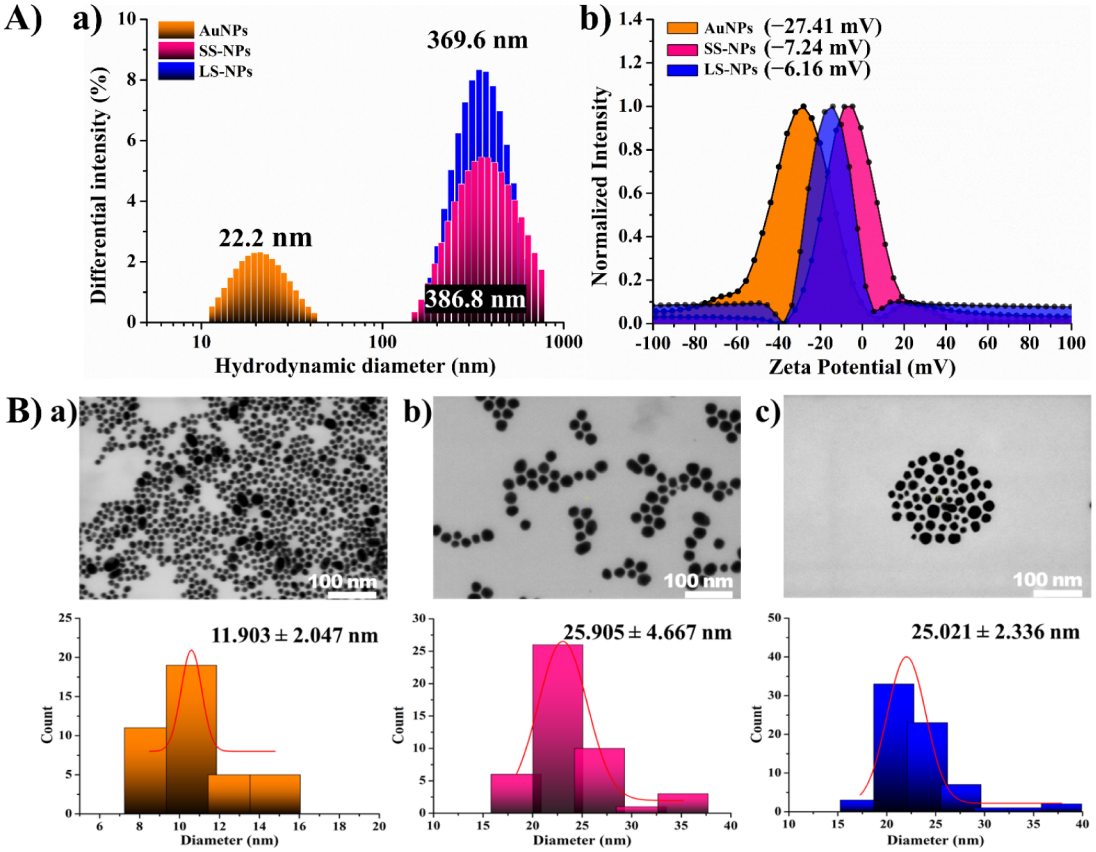

Figure 2. (A) DLS analysis of the gold core of nanoparticles, SS-NPs, and LS-NPs in ultrapure water at an ambient temperature of 25 °C. (a) Overlayed hydrodynamic diameter distributions; (b) overlayed zeta potential plots. Data are presented as mean ± SD (n = 3). (B) STEM imaging of (a) AuNPs, (b) SS-NPs, and (c) LS-NPs. The corresponding size distribution histograms were plotted by measuring the most clearly visible 60 bare gold nanoparticles, SS-NPs, and LS-NPs.

nucleic acids, (iii) a cytotoxicity decreaser composed of a short-chain PEG that acts as an electrostatic shielding/screening layer, and finally (iv) a glucosamine molecule decorating the periphery of the nanoparticle with a tumor-targeting layer. Schematically, the polysegmental structure of the nanoparticle is as follows: **Au_{core}-[PEG_{spacer}-PEI_{linker}-$PEG_{screener}$-$GA_{targeter}$]$_n$**. In order to study the spatiality and to validate the putative functionality of the developed nanoparticles, we built *in silico* models of the nanoconstructs and performed molecular dynamics (MD) simulations to elucidate the intra- and intermolecular interactions that occur between the chain segments in the nanoparticle shell and also between the AuNPs-[PEG-PEI-PEG-GA]$_n$ nanoconstructs and DNA fragments.

RESULTS

The Polysegmental Organization of the Constitutive Chains of the Nanoparticle Shell

To evaluate the impact of the length of the PEG spacer segment on the transfection efficiency of **Au_{core}-[PEG_{spacer}-PEI_{linker}-$PEG_{screener}$-$GA_{targeter}$]$_n$** nanoparticles, we gradually synthesized two types of molecular chains directly grafted onto the Au core, namely (i) **PEG_{2000}-PEG_{500}**-PEI_{2000}-PEG_{500}-GA and (ii) **PEG_{1000}**-PEI_{2000}-PEG_{500}-GA.

The Stepwise Synthesis of the Vectors

First, AuNPs were synthesized and stabilized using sodium citrate. Then, the spacer molecular segment was generated by engrafting a linear α,ω-functionalized PEG molecule having a thiol group in the α position and an amino (HS-PEG_{2000}-**NH_2**) or an oxiranyl (HS-PEG_{1000}-**C_2H_3O**) group, respectively, in the ω position, distinctively for the first and the second vector (see Figure 1). To differentiate the vectors, the spacer segment of the second one was prolonged by using an α,ω-bis-oxiranyl-PEG_{500} precursor. As a third step, the oxiranyl-terminated spacer segment of the shell was subjected to a ring-opening reaction with the primary amine groups of the branched-PEI_{2000} molecules. The reaction concluded by generating the PEI_{linker} segment of the nanoparticle shell, which is the only one capable of complexing polynucleotide chains. In parallel, in order to construct the tail molecular segment, the α,ω-bis-oxiranyl-PEG_{500} precursor was first reacted with GA in a molar ratio of 1:1. Finally, in the fourth step, the -$PEG_{screener}$-$GA_{targeter}$ segment was generated by the reaction between the PEI-terminated shell and the oxiranyl-PEG_{500}-GA tail segment.

For the easy identification of the two vectors which, after the synthesis, differ only by the length of the PEG spacer segment, the following notations will be used in the continuation of the article: (i) for the vector with the structure AuNPs-**PEG_{2000}-PEG_{500}**-PEI_{2000}-PEG_{500}-GA, the notation will be **LS-NPs** (Long Spacer NanoParticles), and (ii) for the vector with the structure AuNPs-**PEG_{1000}**-PEI_{2000}-PEG_{500}-GA, we will use the notation **SS-NPs** (Short Spacer NanoParticles).

FTIR spectrometry was used to confirm the structure of the final compounds (Figure S1). UV−vis spectroscopy (Figure S2 and Table S1), DLS (Table S2), and STEM techniques

https://doi.org/10.1021/acsomega.5c10142
ACS Omega 2026, 11, 4430−4439

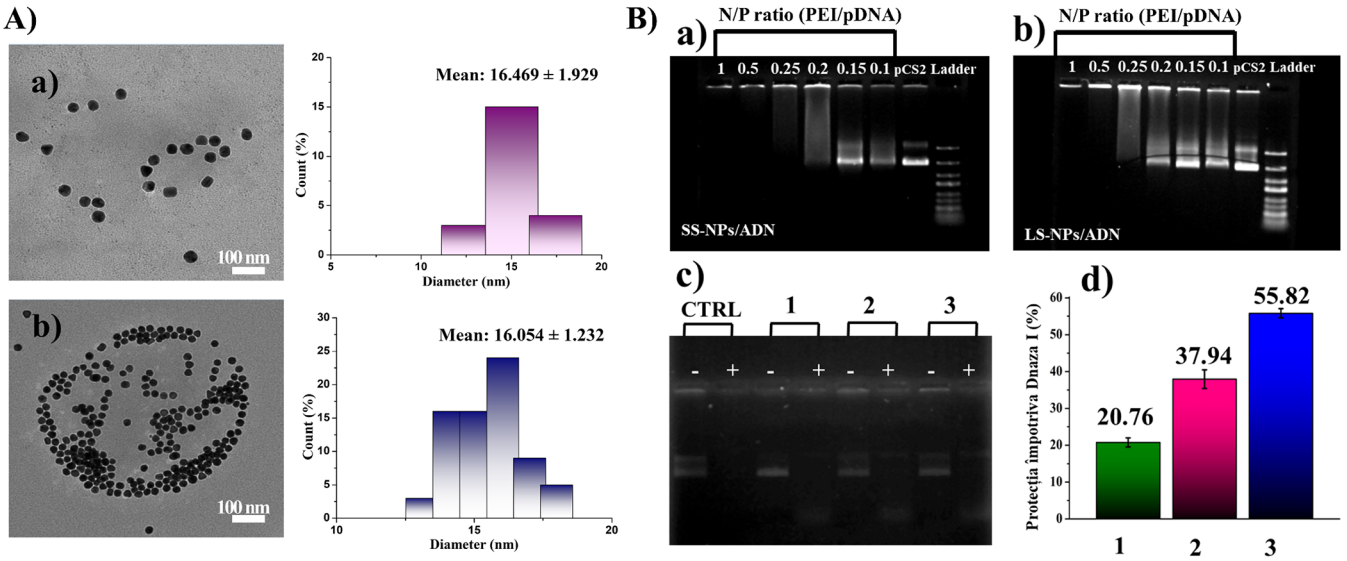

Figure 3. (A) The morphology of the polyplexes generated by the two vectors with plasmid-DNA, as revealed by TEM of (a) SS-NPs/DNA and (b) LS-NPs/DNA polyplexes. (B) Electrophoretic mobility of pCS2 + MT-Luc in the polyplexes formed by (a) SS-NPs and (b) LS-NPs, respectively. Results of the DNase I protection assay (c); representative agarose electrophoresis of polyplexes with pCS2 + MT-Luc incubated in the absence (−) or presence (+) of DNase I, using pCS2 + MT-Luc as a control sample: (**1**) PEI2000, (**2**) SS-NPs, and (**3**) LS-NPs. (d) Quantification of the total of the relaxed and supercoiled electrophoretic plasmid bands corresponding to the pCS2 + MT-Luc samples complexed with (**1**) PEI2000, (**2**) SS-NPs, and (**3**) LS-NPs, after treatment with DNase I (untreated pCS2 + MT-Luc value equal to 100).

(Figure S3) were used to determine the particle's reactivity, morphology, and size. All of the spectra are included in the spectra section of the Supporting Information file.

The Size of Nanoparticles and Their Colloidal Stability in the Liquid Milieu during the Successive Steps of Synthesis

To demonstrate that the vectors were incrementally generated starting from the gold core, DLS analysis was used to estimate the size and colloidal stability by measuring the zeta potential (ζ) of the successively constructed nanoparticles, as shown in Figure 2A and Table S2 of the Supporting Information file. DLS histograms revealed dimensionally uniform assemblies, with a clear increase of their hydrodynamic diameter as a function of the length of the grafted macromolecular chains. In the case of the first vector, the AuNPs-PEG-NH_2 intermediate (ζ = −8.61) had a diameter of 78.7 nm, while the AuNPs-PEG-PEG-C_2H_3O sample (ζ = −12.99) was slightly larger at 91.5 nm. The AuNPs-PEG-PEG-PEI sample (ζ = −4.29) exhibited a larger diameter of 116.5 nm, and the largest diameter, 369.6 nm, was observed for the LS-NP vector (ζ = −7.24). For the second vector (SS-NPs), the AuNPs-PEG-C_2H_3O intermediate (ζ = −13.14) had a hydrodynamic diameter of 71.3 nm. Upon functionalization with PEI, an increase in diameter was observed for AuNPs-PEG-PEI to 118.9 nm (ζ = −8.37). After the final synthesis step, the diameter of the SS-NP vector increased to 386.8 nm (ζ = −6.16). The zeta potential always remains negative and below the colloidal stability threshold (±30 mV), regardless of the stage of synthesis, suggesting that electrostatic repulsion is insufficient to maintain nanoparticles in a stable colloidal suspension.

Dry-State Morphology and the Aggregation Propensity of the Nanoparticulate Vectors

***In Silico* Confirmation by MD.** Morphology was investigated using STEM (Figure 2B) and TEM (Figure 3A) techniques. According to STEM imaging, the nude Au core (Figures 2B.a and S3.a) has a size of 11.9 ± 2.05 nm. After the first PEGylation step, the average diameter of the future SS-NPs and LS-NPs increased to 23.37 ± 3.62 and 21.73 ± 3.27 nm, respectively. The elongation of the spacer segment of LS-NPs resulted in an increase in diameter to 22.89 ± 4.51 nm. Upon further coupling with PEI (Figure S3.c and S3.k), nanoparticles adopted a stable spherical shape and improved dispersibility in water, with their average diameter increasing to 24.76 ± 3.65 nm and 24.24 ± 3.26 nm for SS-NPs and LS-NPs, respectively. After the last synthesis step (peripheral decoration with GA), the vectors displayed a higher tendency for agglomeration and an increase in size (Figure 2B.b and B.c and S3.d and S3.i) to 25.9 ± 4.67 and 25.02 ± 2.33, respectively. The data from the MD simulations are consistent with these findings, as seen in Figure S6, where the radius of the polymeric shell is depicted and has values of 51 and 63 Å for the LS-NPs and SS-NPs, respectively.

TEM images have revealed spherical morphological shapes for both SS-NPs/DNA and LS-NPs/DNA polyplexes (Figure 3A), with an average diameter of approximately 16 nm. As expected, the addition of the plasmid DNA leads to a decrease in the size of the assemblies, a fact that is also explained well by the MD simulations. As can be seen in Figures S4.b and S5.b, the PEI segment is fully extended away from the gold core. However, once the DNA is added (Figures S4.c and S5.c), the PEI bends and collapses onto the DNA fragment, leading to a decrease in the size of the polymeric shell.

Transfection Mediated by the Developed Vectors

Obtaining and Characterizing Polyplexes with Plasmid DNA. The ability of the SS-NPs and LS-NPs to load the pCS2 + MT-Luc plasmid was assessed by agarose gel electrophoresis at different N/P ratios using the naked pCS2 + MT-Luc as a control. In the case of the SS-NP vector, the plasmid DNA is completely loaded at an N/P ratio of 0.25 (Figure 3B.a), whereas in the case of LS-NPs, the polyplexes are completely formed at N/P ratios higher than 0.5 (Figure 3B.b). As expected, the capacity of p-DNA binding is related to

https://doi.org/10.1021/acsomega.5c10142
ACS Omega 2026, 11, 4430−4439

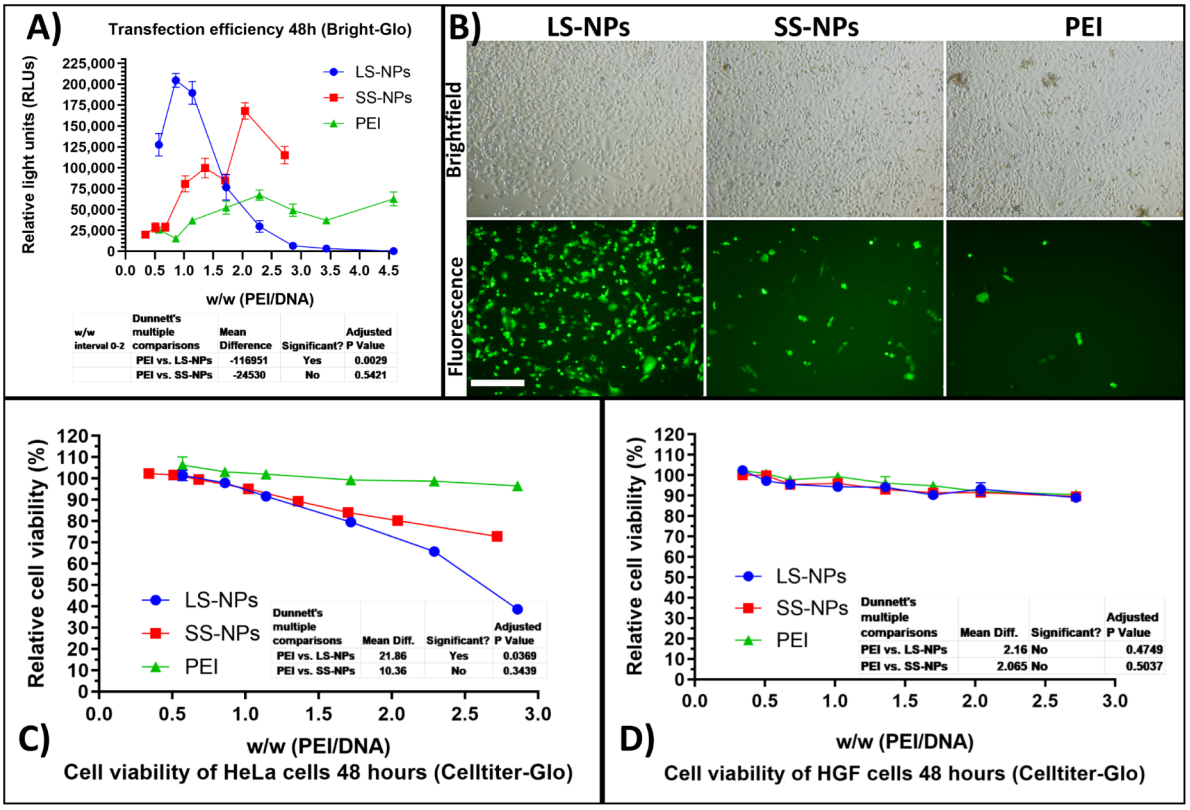

Figure 4. (A) Transfection efficiency of LS-NPs, SS-NPs, and PEI_{2000} with the pCS2 + MT-Luc polyplexes on HeLa cells. HeLa cells were seeded in opaque white 96-well plates, 1×10^4 cells/well, and were transfected with polyplexes in various mass ratios (mass of the PEI segment of the vector/mass of the plasmid). After 48 h from the transfection, the samples were treated with 100 μL Bright-Glo reagent each, and the emitted light was read. (B) Fluorescence microscopy of transfected HeLa cells. HeLa cells were cultured in several 5×10^4 cells per well, in 24-well plates, and transfected with polyplexes containing 2500 ng of pCS2 + NLS-eGFP plasmid. The w/w ratio PEI weight/pDNA weight was 1 for LS-NPs, 2 for SS-NPs, and 2 for PEI_{2000}. Cells were photographed under a microscope using the GFP filter, 48 h after transfection. The scale bar is 200 μm. CellTiter-Glo viability assay on (C) HeLa and (D) HGF cell lines. The cells were seeded in opaque white 96-well plates, 1×10^4 cells/well for HeLa cells and 5×10^3 cells/well for HGF cells, and were transfected with polyplexes in various mass ratios (mass of the PEI segment of the vector/mass of the plasmid).

the length of the PEG spacer chain,[19] considering that the molecular weight of the spacer segment of SS-NPs is 2.5 times lower than that of the LS-NP vector.

The ability of PEI_{2000}, SS-NPs, and LS-NPs to safeguard plasmid DNA from endonuclease degradation (Figure 3B.c and B.d) was assessed by forming polyplexes at an N/P ratio of 0.5 when the PEI content was kept constant at 0.34 mg/mL. As revealed by Figure 3B.c, the vectors and the naked PEI provide good protection of plasmid DNA against the action of DNase I. After the incubation of DNase I-treated polyplexes with SDS (Figure 3B.d), PEI_{2000}, SS-NPs, and LS-NPs, respectively, released 20.76%, 37.94%, and 5.82% of the incubated plasmid DNA. LS-NP conjugate, however, preserved the highest amount of plasmid content, followed by the SS-NPs, and finally, the lowest protection capacity of plasmid DNA was measured in the case of branched PEI_{2000} macromolecules. The ability of the studied vectors to protect DNA is due to the insertion of DNA into their bulky polymeric periphery, as seen in Figures S4.c and S5.c, where DNA is immersed into the PEI moiety.

Qualitative and Quantitative Evaluation of In Vitro Transfection Efficiency Conducted on HeLa Cell Cultures. First, the transfection efficiency of LS-NPs, SS-NPs, and PEI2000 with the pCS2 + MT-Luc polyplexes was performed according to Figure 4A. For the qualitative evaluation, polyplexes were made with the plasmid pCS2 + NLS + eGFP, which contains the gene for an enhanced green fluorescent protein, as illustrated in Figure 4A. Observations at 48 h post-treatment indicated that the transfection efficiency varied significantly with the structural length of the vectors. The LS-NP vector exhibited a markedly enhanced eGFP expression compared to the shorter vector, SS-NPs. The difference in PEG spacer length appeared to represent a critical factor influencing transfection potency. Moreover, both vectors, regardless of their PEG spacer length, achieved stronger transfection levels than the free PEI control, highlighting the importance of AuNPs' derivatization in enhancing gene delivery efficiency. This indicates that not only does the PEG spacer play a pivotal role, but the presence of the AuNPs' core itself is essential for achieving superior transfection performance.

Qualitative observations were further validated through a quantitative assessment of transfection efficiency using LS-NPs/DNA, SS-NPs/DNA, and PEI_{2000}/DNA polyplexes, all loaded with the pCS2 + MT-Luc plasmid encoding luciferase. The Bright-Glo assay was employed to quantify luciferase expression in HeLa cells following transfection with these polyplexes (Figure 4B). The results revealed that the vectors demonstrated varying transfection efficiencies, with LS-NPs (Figure 4B) showing a notably higher transfection rate

https://doi.org/10.1021/acsomega.5c10142
ACS Omega 2026, 11, 4430−4439

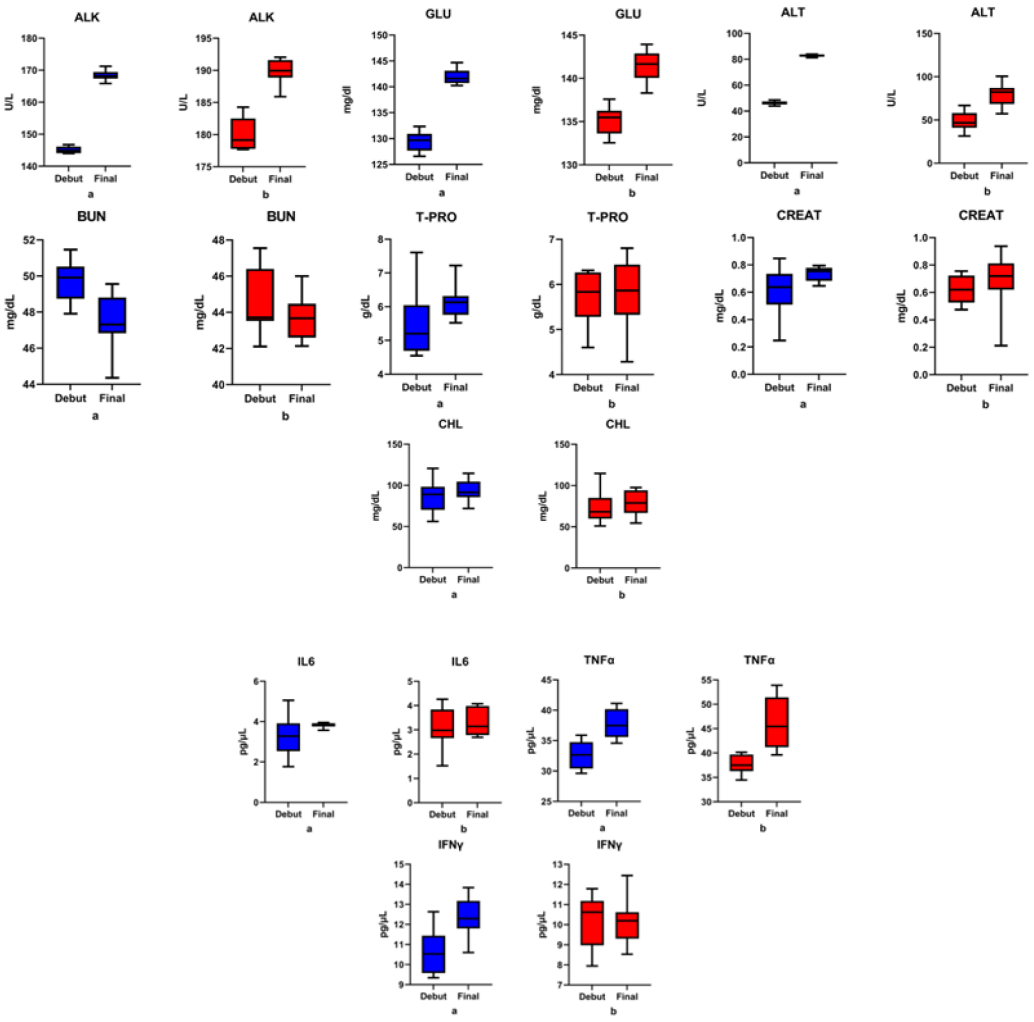

Figure 5. Graphical evolution of biochemical markers and IL-6, TNFα, and IFNγ in BALB/c mice to the administration of (a) LS-NP (blue color) and (b) SS-NP conjugates (red color).

compared to SS-NPs (Figure 4B) and free PEI (Figure 4B). For w/w up to 2, the efficiency of LS-NPs is statistically significantly higher than that of PEI and SS-NPs. Also, in the same interval, the efficiency of SS-NPs is higher than that of PEI, but not statistically significant. This suggests that the increased length of the PEG spacer enhances gene delivery effectiveness.

Furthermore, the optimal transfection efficiency for each vector was achieved at distinct mass ratios, emphasizing the importance of the PEG spacer length in determining the ideal polyplex configuration. Specifically, the LS-NP vector achieved peak efficiency at a w/w ratio of approximately 1, while the SS-NP vector was more effective at a higher w/w ratio of 2. These findings suggest that tuning the PEG chain length and optimizing the mass ratio are both crucial for maximizing transfection performance, potentially allowing for customizable gene delivery systems based on PEG chain design.

Cell Viability. Polyplexes bearing the pCS2 + NLS-eGFP plasmid were evaluated for cytotoxicity and biocompatibility on HeLa (cancerous) and HGF (noncancerous) cell lines using the CellTiter-Glo Luminescent Cell Viability Assay (Figure 4C and D). This assay leverages luciferase−luciferin chemistry to generate light in the presence of adenosine triphosphate (ATP), a marker of metabolically active cells, allowing for a direct assessment of cell viability based on light intensity. The experiments to evaluate the cytotoxicity of the transfection *in vitro* on the HeLa cell line (Figure 4C, D) utilized LS-NPs/DNA, SS-NPs/DNA, and PEI2000/DNA polyplexes with pCS2 + NLS-eGFP. The data showed that LS-NPs/DNA polyplexes exhibited slightly higher but statistically significant cytotoxicity across all tested concentrations compared to SS-NPs/DNA ones. This increased cytotoxicity may be attributed to enhanced cellular uptake or increased interaction with cellular membranes, which are influenced by the longer PEG spacer. Interestingly, on the HGF cell line (Figure 4D), both polyplexes demonstrated very low cytotoxicity, statistically not significant, with cell viability remaining high across all concentrations. This suggests that the polyplexes, particularly those with LS-NPs, may selectively affect cancer cells more than noncancerous cells, potentially offering a balance of transfection efficiency with biocompatibility in nontarget cells.

Analysis of transfection efficiency data led us to conclude that positioning a longer PEG chain adjacent to the AuNPs' core offers significant advantages in enhancing the transfection efficiency in HeLa cancer cells. The increased PEG length appears to improve cellular uptake and vector stability, suggesting that careful control of the PEG spacer length can optimize gene delivery performance for cancer cell applications.

https://doi.org/10.1021/acsomega.5c10142
ACS Omega 2026, 11, 4430−4439

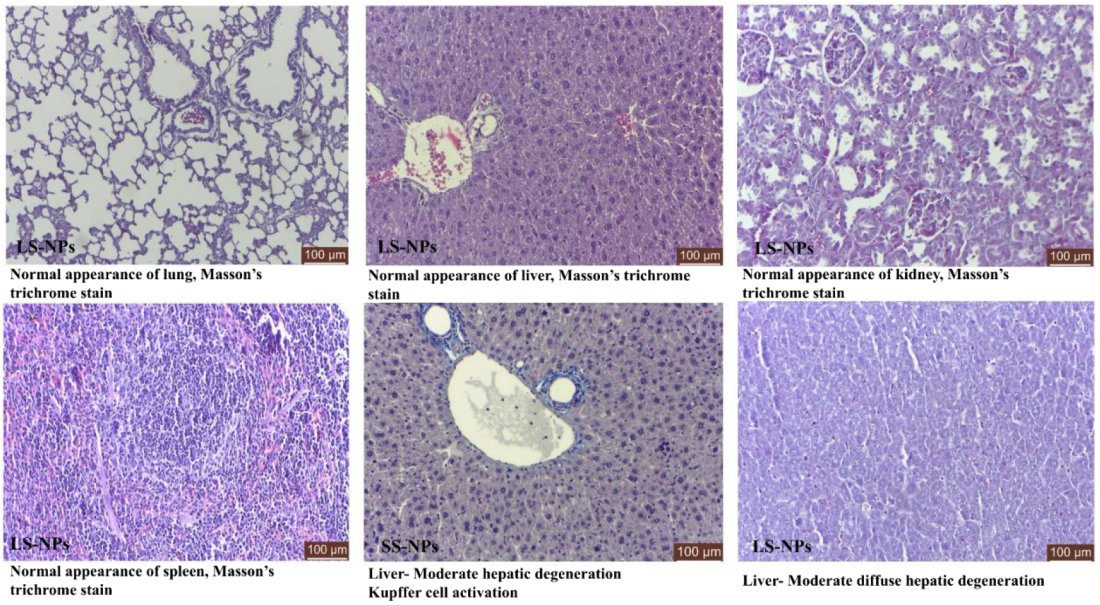

Figure 6. Histological changes in the liver of BALB/c mice after the administration of LS-NP and SS-NP vectors.

Evaluation of Toxicity (Acute-LD_{50} and Repeated Doses). In the LS-NP group, 50% of the animals survived after receiving a single dose of 6 mg/mouse. In the SS-NP group, LD_{50} was determined to be 1.90 mg/mouse. Throughout the monitoring period, the surviving animals in both groups did not exhibit any behavioral changes or signs of toxicity. After determining the toxicity at repeated doses of the two vectors, no behavioral changes, differences in body weight, or other signs of late clinical toxicity were observed. Mice have maintained their interest in food and water during the 7 days of monitoring. Also, no cases of mortality have been registered (Table S3 from the Supporting Information).

Hematological Analyses. The evolution of the hematological parameters is presented in Tables S4 and S5 from the Supporting Information. The evaluated parameters did not have significant changes that would attribute an inflammatory effect to the LS-NP and SS-NP vector. At the same time, at the end of the 7 days of testing, the average values of the hematological indices and those of the platelets indicate minor differences in both groups compared to the beginning of the experiment; these values correspond to the physiological interval of this line of mice (BALB/c).[21]

Biochemical Analyses. The analysis of the biochemical parameters in the blood is a method of monitoring renal (BUN and CREAT) and hepatic (ALT, ALP, PT) functions for the evaluation of new molecules through toxicological studies or the diagnosis of induced metabolic disorders (GLU, CHOL). In general, inorganic compounds can induce an inflammatory response and alter biochemical indices. In Figure 5, we highlighted in color blue LS-NP vector, while e SS-NP vector is shown in color red. In the case of both vectors, the values of BUN, GLU, and ALK were higher compared with those at the beginning of the experiment, but they evolved between the physiological values in this line of mice. However, the significant variation of ALT in the two groups, LS-NPs and SS-NPs, indicates possible liver distress. No changes in serum cholesterol or creatinine levels were observed. The data are presented in Tables S6 from the Supporting Information.

The evaluation of the serum levels of IL6 (interleukin 6), TNFα (tumor necrosis factor alpha), and IFNγ (interferon-gamma) in the two groups shows a slightly increased level in the LS-NP group compared to the SS-NPs, which indicates the presence of moderate acute inflammation in the liver but not in other organs. The serum levels of the analyzed cytokines are presented in Figure 5 and Table S7 from the Supporting Information.

Histopathological Examination. For both vectors, reversible morphological changes were observed only in the liver, manifested by moderate liver degeneration, with Kupffer cell activation in 3 from 10 mice for compound LS-NPs and in 2 from 10 mice for vector SS-NPs. The presence of binucleated cells indicates the existence of an ongoing regeneration process (Figure 6). No other changes, such as atrophy, congestion, shape, volume, or color, were observed. Other organs, such as the lungs, kidneys, and spleen, were not affected and presented a normal appearance in the histological sections.

Intravenous administration to BALB/c mice of the two vectors, three times within a week, did not induce clinical signs of toxicity, such as ruffled fur, inability to move, incoordination of movements, or respiratory or digestive impairment. The behavior of the animals was normal, and the weight did not vary significantly; the animals maintained their appetite for food and water. Moreover, no changes were recorded in the examined indices (hematological, biochemical, and immunological), although the direct influence of the vectors on these indices was signaled by changes in the parameters that can induce an inflammatory response and alterations in the number of blood cells.[22,23]

Histologically, no changes of an inflammatory nature were observed in the spleen, lung, and kidney. A slight liver degeneration, with Kupffer cell activation, was recorded for both vectors, but the presence of binucleated cells indicates a transient, reversible process that does not influence the health status of the laboratory animals (Figure S9). Kupffer cell activation is responsible for the early stage damage to the liver, which is the main organ involved in the biotransformation of gold nanoparticles.[24] A marker of this recorded liver distress is

https://doi.org/10.1021/acsomega.5c10142
ACS Omega 2026, 11, 4430−4439

ALT (alanine-amino-transferase), which showed a slight increase in serum levels at the end of the experiment, in both vectors, but which is within the normal parameters of this mouse line.[21] The physiological serum variations of the biochemical indices BUN, GLU, and TPO indicate activation of the metabolism, with a role in local defense, sequestration, and renal excretion of the two vectors. Previous studies have reported that gold nanoparticles can induce renal damage, effects that can be exacerbated by interaction with drugs or other chemicals.[25] In our study, no significant changes in the biochemical markers of renal function (BUN and CREAT) were observed. Also, renal lesions such as twisted glomeruli, edema, necrosis, and inflammatory infiltrates were not observed, although biologically, females are more prone to develop adverse effects to various chemical agents or drugs, through a different male−female endocrine regulatory mechanism of the enzymatic pathways of drug biotransformation.[26−28] There is a high probability that renal diseases are associated with elevated concentrations and smaller sizes of gold nanoparticles, which may be correlated with the route of administration.[25,29] One of the biological actions of TNF-α at the cellular level is to induce the synthesis of other cytokines, of some enzymes involved in the production of some pro-inflammatory mediators, or acute phase proteins.[30] TNF-α shows elevated serum levels in many acute and chronic liver diseases induced by exposure of the liver to various chemicals or drugs. The presence of this interleukin is linked to the repair process by regulating the release of other mediators involved in the healing of the inflammatory process.[31] The increased serum level of TNF-α should not necessarily be interpreted as a mediator of liver inflammation but rather as having an important role in establishing the function of this organ by stimulating hepatocyte proliferation and liver regeneration. TNF-α activates several intracellular pathways to regulate inflammation, cell death, and proliferation. Decreased hepatocyte proliferation shows that IKK-β (Ikappaβ kinase) exerts specific functions in liver cell populations. In hepatocytes, it protects against TNF-induced apoptosis, and in Kupffer cells, IKK-β induces transcription of proinflammatory and proliferative mediators.[32] These results are interesting in the clinical context of liver diseases involving the activation of Kupffer cells.

Considering these results, repeated intravenous administration of the two vectors is safe; all animals involved in the experiment survived without alteration of their health status. Changes in biochemical (especially ALT) and immunological (TNFα) indices express slight liver damage, but it is reversible and not always of an inflammatory nature (it can be a process of regulating enzyme function). The data obtained for the two vectors do not prove the existence of significant differences regarding their toxicity in intravenous administration and provide a strong reason to consider a clinical-therapeutic approach.

DISCUSSION

In this study, we report the design, synthesis, characterization, and *in vitro* translated to *in vivo* evaluation, corroborated with *in silico* studies of two novel polymer-saccharide-functionalized gold nanoparticles capable of acting as nonviral vectors with potential applications in targeted gene therapy of tumor cells. The studied nanoparticles are of a multishell type, with the periphery decorated with glucosamine molecules. They are generated by grafting PEG and PEI polymeric chains onto a core of gold atoms and differ from each other by the length of the PEG segments acting as spacers located between the Au core and a branched PEI moiety, the latter being the one directly involved in nucleic acid transport processes. The positioning and the length of PEG segments modulate the gene-transporting performance of the nanoparticles, and the decoration with glucosamine allows them to selectively target tissue domains and cells with high glucose consumption, such as tumors and neoplastic cells.

The novelty of this type of multicomponent multishell nanoparticles consists in (i) the ease with which they can be synthesized and (ii) the versatility of structuring the shells, a fact translated into the possibility of "by design" tailoring of their functional performances as gene vectors. Moreover, the presence, sequence, and length of the PEG spacer located in the immediate vicinity of the gold core ensure minimal toxicity to nontumor cells (tested on the HGF cell line) and lack of systemic toxicity (demonstrated by intravenous administration studies on BALB/c mice), thus avoiding the disadvantages noted for other types of nanoparticulate nonviral gene vectors, including those built around AuNPs.

Overall, the nanoparticles developed by us offer an improvement in transfection efficiency in the context of insignificant recruitment of immune cells, as reflected by the lack of inflammatory reactions and the lack of damage to the internal organs of laboratory mice. The improved biocompatibility and carrying and targeting ability of the AuNPs-(PEG_x)-PEG_y-PEI_{2000}-PEG_{500}-GA nanoparticles provide a strong reason to consider a further clinical-therapeutic approach.

MATERIALS AND METHODS

Gold precursors, citrate, PEG derivatives, PEI, glucosamine, and all cell-culture reagents were purchased from commercial suppliers and used as received. HeLa and HGF cell lines were cultured under standard conditions. BALB/c mice were maintained and treated according to EU Directive 63/2010 and institutional ethical approval.

Gold nanoparticles were synthesized by a modified Turkevich method and subsequently functionalized with PEG, PEI, and GA-PEG to obtain LS-NPs and SS-NPs. Nanoparticles were characterized by UV−vis spectroscopy, DLS, STEM/TEM, and FTIR. The PEI content was determined by UV−vis using a $CuCl_2$ complex assay.

Polyplexes were prepared at defined N/P ratios and assessed by agarose gel electrophoresis and DNase I protection assays. Transfection efficiency (luciferase and eGFP reporters) and cytotoxicity (CellTiter-Glo) were evaluated in HeLa and HGF cells.

In vivo toxicity was assessed through acute and repeated-dose studies, followed by hematological, biochemical, immunological, and histopathological analyses. Statistical significance was determined using ANOVA-based tests. Molecular dynamics simulations of nanoparticle−DNA interactions were performed with GROMACS under NPT conditions.

Comprehensive descriptions of all experimental and analytical methods are available in the Supporting Information.

https://doi.org/10.1021/acsomega.5c10142
ACS Omega 2026, 11, 4430−4439

■ ASSOCIATED CONTENT

Data Availability Statement

The raw/processed data required to reproduce these findings cannot be shared at this time due to technical or time limitations.

Supporting Information

The Supporting Information is available free of charge at https://pubs.acs.org/doi/10.1021/acsomega.5c10142.

Experimental details and comprehensive data; full descriptions of the materials, methods, and experimental procedures; supplementary figures and tables; FTIR and UV−vis spectroscopy analyses; colloidal characterization of the developed nonviral gene vectors and their intermediates (including UV−vis, DLS, zeta potential, and STEM data); morphological assessments; *in silico* modeling and simulation results; and extended in vivo evaluation data, including toxicity studies (acute LD50 and repeated-dose assessments), hematological and biochemical analyses, and detailed histopathological examinations (PDF)

■ AUTHOR INFORMATION

Corresponding Authors

Cristina M. Al-Matarneh − *Centre of Advanced Research in Bionanoconjugates and Biopolymers, "Petru Poni" Institute of Macromolecular Chemistry of Romanian Academy, Iasi 700487, Romania;* orcid.org/0000-0001-9299-1347; Email: almatarneh.cristina@icmpp.ro

Mariana Pinteala − *Centre of Advanced Research in Bionanoconjugates and Biopolymers, "Petru Poni" Institute of Macromolecular Chemistry of Romanian Academy, Iasi 700487, Romania;* orcid.org/0000-0002-4021-982X; Email: pinteala@icmpp.ro

Authors

Denisse I. Bostiog − *Centre of Advanced Research in Bionanoconjugates and Biopolymers, "Petru Poni" Institute of Macromolecular Chemistry of Romanian Academy, Iasi 700487, Romania*

Valentin Nastasa − *Laboratory of Antimicrobial Chemotherapy, Faculty of Veterinary Medicine, "Ion Ionescu de la Brad" Iasi University of Life Sciences, Iasi 700489, Romania;* orcid.org/0000-0001-7384-8692

Dragos Peptanariu − *Centre of Advanced Research in Bionanoconjugates and Biopolymers, "Petru Poni" Institute of Macromolecular Chemistry of Romanian Academy, Iasi 700487, Romania*

Mihai Mares − *Laboratory of Antimicrobial Chemotherapy, Faculty of Veterinary Medicine, "Ion Ionescu de la Brad" Iasi University of Life Sciences, Iasi 700489, Romania*

Sorin A. Pasca − *Laboratory of Antimicrobial Chemotherapy, Faculty of Veterinary Medicine, "Ion Ionescu de la Brad" Iasi University of Life Sciences, Iasi 700489, Romania*

Andra C. Bostanaru-Iliescu − *Laboratory of Antimicrobial Chemotherapy, Faculty of Veterinary Medicine, "Ion Ionescu de la Brad" Iasi University of Life Sciences, Iasi 700489, Romania*

Bogdan F. Craciun − *Centre of Advanced Research in Bionanoconjugates and Biopolymers, "Petru Poni" Institute of Macromolecular Chemistry of Romanian Academy, Iasi 700487, Romania;* orcid.org/0000-0002-2324-0088

Tudor Vasiliu − *Centre of Advanced Research in Bionanoconjugates and Biopolymers, "Petru Poni" Institute of Macromolecular Chemistry of Romanian Academy, Iasi 700487, Romania*

Razvan Puf − *Centre of Advanced Research in Bionanoconjugates and Biopolymers, "Petru Poni" Institute of Macromolecular Chemistry of Romanian Academy, Iasi 700487, Romania*

Stelian S. Maier − *Centre of Advanced Research in Bionanoconjugates and Biopolymers, "Petru Poni" Institute of Macromolecular Chemistry of Romanian Academy, Iasi 700487, Romania; SMART-Tex-IS Research Center, "Gheorghe Asachi" Technical University of Iasi, Iasi 700050, Romania*

Complete contact information is available at: https://pubs.acs.org/10.1021/acsomega.5c10142

Author Contributions

#D.I.B. and V.N. made equal contributions. Synthesis, physicochemical characterization, and results writing: D.I.B., C.M.A.-M., B.F.C.; *in vitro* and *in vivo* assessments and results writing: V.N., D.P., M.M., S.A.P., A.C.B.-I.; *in silico* characterization and results writing: T.V., R.P.; conceptualization, data interpretation, and manuscript writing: S.S.M., M.P. All authors gave final approval and agreed to be accountable for all aspects of the work.

Notes

The authors declare no competing financial interest.

■ ACKNOWLEDGMENTS

This paper is supported by the European Union's Horizon Europe Research and Innovation Program under grant agreement No. 101086667, project BioMat4CAST (BioMat4-CAST—"Petru Poni"Institute of Macromolecular Chemistry Multiscale *In Silico* Laboratory for Complex and Smart Biomaterials), and grants of computing time from the Swedish National Infrastructure for Computing (SNIC at PDC) are gratefully acknowledged.

■ REFERENCES

(1) Yücel, A. D.; Gladyshev, V. N. The Long and Winding Road of Reprogramming-Induced Rejuvenation. *Nat. Commun.* **2024**, *15* (1), 1941.

(2) Wang, R.; Duan, X.; Li, J.; Zhang, C.; Shen, L. Emerging Strategies of Cell and Gene Therapy Targeting Tumor Immune Microenvironment. *Clin. Cancer Res.* **2025**, *31* (12), 2294−2308.

(3) Pensotti, A.; Bertolaso, M.; Bizzarri, M. Is Cancer Reversible? Rethinking Carcinogenesis Models—A New Epistemological Tool. *Biomolecules* **2023**, *13* (5), 733.

(4) Hosseinkhani, H.; Domb, A. J.; Sharifzadeh, G.; Nahum, V. Gene Therapy for Regenerative Medicine. *Pharmaceutics* **2023**, *15* (3), 856.

(5) Vogt, N. A Light Switch for Kinases. *Nat. Methods* **2017**, *14* (5), 466−467.

(6) Ginn, S. L.; Amaya, A. K.; Alexander, I. E.; Edelstein, M.; Abedi, M. R. Gene Therapy Clinical Trials Worldwide to 2017: An Update. *J. Gene Med.* **2018**, *20* (5), No. e3015.

(7) Zoefel, B.; VanRullen, R. The Role of High-Level Processes for Oscillatory Phase Entrainment to Speech Sound. *Front. Hum. Neurosci.* **2015**, *9*, 651.

(8) Du, T.; Zhou, G.; Roizman, B. Induction of Apoptosis Accelerates Reactivation of Latent HSV-1 in Ganglionic Organ Cultures and Replication in Cell Cultures. *Proc. Natl. Acad. Sci.* **2012**, *109* (36), 14616−14621.

(9) Yudaeva, A.; Kostyusheva, A.; Kachanov, A.; Brezgin, S.; Ponomareva, N.; Parodi, A.; Pokrovsky, V. S.; Lukashev, A.; Chulanov, V.; Kostyushev, D. Clinical and Translational Landscape of Viral Gene Therapies. *Cells* **2024**, *13* (22), 1916.
(10) Wang, C.; Pan, C.; Yong, H.; Wang, F.; Bo, T.; Zhao, Y.; Ma, B.; He, W.; Li, M. Emerging Non-Viral Vectors for Gene Delivery. *J. Nanobiotechnol.* **2023**, *21* (1), 272.
(11) Jones, A. K.; Buckingham, S. D.; Sattelle, D. B. Chemistry-to-Gene Screens in Caenorhabditis Elegans. *Nat. Rev. Drug Discovery* **2005**, *4* (4), 321−330.
(12) Hoare, J.; Waddington, S.; Thomas, H. C.; Coutelle, C.; McGarvey, M. J. Complement Inhibition Rescued Mice Allowing Observation of Transgene Expression Following Intraportal Delivery of Baculovirus in Mice. *J. Gene Med.* **2005**, *7* (3), 325−333.
(13) Lv, H.; Zhang, S.; Wang, B.; Cui, S.; Yan, J. Toxicity of Cationic Lipids and Cationic Polymers in Gene Delivery. *J. Controlled Release* **2006**, *114* (1), 100−109.
(14) Knop, K.; Hoogenboom, R.; Fischer, D.; Schubert, U. S. Poly(Ethylene Glycol) in Drug Delivery: Pros and Cons as Well as Potential Alternatives. *Angew. Chemie Int. Ed.* **2010**, *49* (36), 6288−6308.
(15) Kao, T.; Kohle, F.; Ma, K.; Aubert, T.; Andrievsky, A.; Wiesner, U. Fluorescent Silica Nanoparticles with Well-Separated Intensity Distributions from Batch Reactions. *Nano Lett.* **2018**, *18* (2), 1305−1310.
(16) Mitchell, M. J.; Billingsley, M. M.; Haley, R. M.; Wechsler, M. E.; Peppas, N. A.; Langer, R. Engineering Precision Nanoparticles for Drug Delivery. *Nat. Rev. Drug Discovery* **2021**, *20* (2), 101−124.
(17) Danhier, F.; Ansorena, E.; Silva, J. M.; Coco, R.; Le Breton, A.; Préat, V. PLGA-Based Nanoparticles: An Overview of Biomedical Applications. *J. Controlled Release* **2012**, *161* (2), 505−522.
(18) Craciun, B. F.; Gavril, G.; Peptanariu, D.; Ursu, L. E.; Clima, L.; Pinteala, M. Synergistic Effect of Low Molecular Weight Polyethylenimine and Polyethylene Glycol Components in Dynamic Nonviral Vector Structure, Toxicity, and Transfection Efficiency. *Molecules* **2019**, *24* (8), 1460.
(19) Craciun, B. F.; Clima, L.; Bostiog, D.-I.; Silion, M.; Calin, M.; Peptanariu, D.; Pinteala, M. Multilayer Gold Nanoparticles as Non-Viral Vectors for Targeting MCF-7 Cancer Cells. *Biomater Adv.* **2023**, *144*, 213201.
(20) Clima, L.; Peptanariu, D.; Pinteala, M.; Salic, A.; Barboiu, M. DyNAvectors: Dynamic Constitutional Vectors for Adaptive DNA Transfection. *Chem. Commun.* **2015**, *51* (99), 17529−17531.
(21) Colonies *BALB/C Nude Mouse*; Charles river, 2008.
(22) Hauck, T. S.; Anderson, R. E.; Fischer, H. C.; Newbigging, S.; Chan, W. C. W. In Vivo Quantum-Dot Toxicity Assessment. *Small* **2010**, *6* (1), 138−144.
(23) Gjetting, T.; Arildsen, N. S.; Christensen, C. L.; Poulsen, T. T.; Roth, J. A.; Handlos, V. N.; Poulsen, H. S. In Vitro and in Vivo Effects of Polyethylene Glycol (PEG)-Modified Lipid in DOTAP/Cholesterol-Mediated Gene Transfection. *Int. J. Nanomed.* **2010**, *5* (1), 371−383.
(24) Balasubramanian, S. K.; Jittiwat, J.; Manikandan, J.; Ong, C.-N.; Yu, L. E.; Ong, W.-Y. Biodistribution of Gold Nanoparticles and Gene Expression Changes in the Liver and Spleen after Intravenous Administration in Rats. *Biomaterials* **2010**, *31* (8), 2034−2042.
(25) Isoda, K.; Tanaka, A.; Fuzimori, C.; Echigoya, M.; Taira, Y.; Taira, I.; Shimizu, Y.; Akimoto, Y.; Kawakami, H.; Ishida, I. Toxicity of Gold Nanoparticles in Mice Due to Nanoparticle/Drug Interaction Induces Acute Kidney Damage. *Nanoscale Res. Lett.* **2020**, *15* (1), 141.
(26) Ibrahim, K. E.; Al-Mutary, M. G.; Bakhiet, A. O.; Khan, H. A. Histopathology of the Liver, Kidney, and Spleen of Mice Exposed to Gold Nanoparticles. *Molecules* **2018**, *23* (8), 1848.
(27) Nicolson, T. J.; Mellor, H. R.; Roberts, R. R. A. Gender Differences in Drug Toxicity. *Trends Pharmacol. Sci.* **2010**, *31* (3), 108−114.
(28) Miller, M. A. Gender-Based Differences in the Toxicity of Pharmaceuticals - The Food and Drug Administration's Perspective. *Int. J. Toxicol.* **2001**, *20* (3), 149−152.
(29) Zhang, X. D.; Wu, H. Y.; Wu, D.; Wang, Y. Y.; Chang, J. H.; Zhai, Z. B.; Meng, A. M.; Liu, P. X.; Zhang, L. A.; Fan, F. Y. Toxicologic Effects of Gold Nanoparticles in Vivo by Different Administration Routes. *Int. J. Nanomed.* **2010**, *2010*, 771−781.
(30) Kitagawa, Y. Tabes Dorsalis. *Ryoikibetsu Shokogun Shirizu.* **1999**, No. 23 Pt 1, 324−325.
(31) Zhao, S.; Jiang, J.; Jing, Y.; Liu, W.; Yang, X.; Hou, X.; Gao, L.; Wei, L. The Concentration of Tumor Necrosis Factor-α Determines Its Protective or Damaging Effect on Liver Injury by Regulating Yap Activity. *Cell Death Dis.* **2020**, *11* (1), 70.
(32) Schwabe, R. F.; Bradham, C. A.; Uehara, T.; Hatano, E.; Bennett, B. L.; Schoonhoven, R.; Brenner, D. A. C-Jun-N-Terminal Kinase Drives Cyclin D1 Expression and Proliferation during Liver Regeneration. *Hepatology* **2003**, *37* (4), 824−832.

https://doi.org/10.1021/acsomega.5c10142
ACS Omega 2026, 11, 4430−4439